Linear Quadratic Regulator Controller and Observer for Controlling Transient Oscillations near Resonance in Non-Colocated Compliant Mechanism System

Siddhesh Chaudhari[1] and Prasanna Gandhi[2](Member, IEEE)

***Abstract*— Maintaining steady oscillations is a requirement for several electromechanical systems such as oral cavity scanners, mechanical object scanners, micro mirror scanners, etc. In this paper, we consider a scanning system based on non-colocated double parallelogram compliant mechanism. The system is idealized as two springs two masses damper system with end mass as the desired stage. The non-colocated actuation is given only to the intermediate mass and goal is to keep the desired end mass in steady oscillations. Under low damping in the system, traditional open loop sinusoidal excitation given as input results in prolonged (more than 100 s) transient response. Moreover, it would take similar long time to recover from even a small ambient disturbance. We propose here a Linear Quadratic Regulator (LQR) controller along with an observer to overcome this problem. The proposed controller is evaluated through simulation and experimental verification. Experiments are carried out on a double parallelogram resonant displacement amplifying compliant mechanism designed and developed in-house. Along with being robust, effective in disturbance rejection, the proposed control algorithm also features low computational complexity, making it highly suitable for real-time implementation.**

I. Introduction

Maintaining steady oscillations is crucial for various electromechanical applications such as oral cavity scanners, mechanical object scanners, micro mirror scanners, and other precision positioning mechanisms [1] [2]. In this paper, we focus on a non-colocated compliant mechanism, which is described in detail later. Compliant mechanisms have been widely adopted in precision microfabrication applications [3], [4], demonstrating the potential for high-resolution positioning and alignment, ensuring smooth, repeatable, and backlash-free motion. A system is termed *non-colocated* when the point of actuation and the point of measurement or control objective are spatially separated. This causes additional challenges such as phase lags and increased sensitivity to disturbances, making precise control more difficult [5].

The mechanism considered is a double parallelogram compliant system as shown in Fig. 1. It has two assemblies (which can be considered as blocks for this study) connected to each other using a pair of compliant beams; and one of these assemblies is connected to the ground using a second pair of compliant beams. In this way, the system resembles a two-mass spring-damper system connected to the ground on one end. Furthermore, an actuator is attached to the block that is directly connected to the ground via a pair of compliant beams. However, the encoder is placed on the end block, and the motion of this block will be considered of interest throughout the paper. The paper aims to bring this block into steady oscillations quickly and further reject any disturbances.

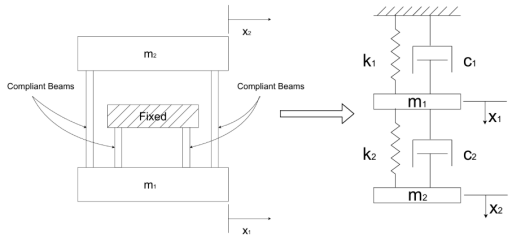

Fig. 1. Double parallelogram compliant mechanism and the corresponding two-mass spring-damper model

The damping in the considered mechanism is very low, which is desirable for many applications. However, this also means that the time taken to reach a steady state from starting from zero initial conditions and recovering from unknown disturbances is high. Simulations show that with a conventional sinusoidal control applied to this system, it takes more than 100 seconds to recover from the transient response. Moreover, any disturbance from the environment after reaching steady state will also require a long recovery time, significantly affecting system performance [6].

Secondly, for practical applications of this mechanism, excitation near its resonance helps achieve large amplitude oscillations with lower energy input, making it highly efficient for periodic tasks like scanning and micro-positioning. However, operating near resonance also increases the system's sensitivity to disturbances, necessitating a robust control strategy [7].

To develop a control strategy that can effectively address the above issues, this non-colocated double parallelogram compliant mechanism is modeled as a two-mass, two-spring, and two-damper system, where actuation is applied to an intermediate mass and the goal is to regulate oscillations of the end mass. We propose an observer-based Linear Quadratic Regulator (LQR) control strategy that optimally

*This work is supported partially by Abdul Kalam Technology Innovation National fellowship under grant no RD/0122-INFLS30-001

[1]Siddhesh Chaudhari is with the Department of Mechanical Engineering, Indian Institute of Technology Bombay, Mumbai, India 210100146@iitb.ac.in

[2]Prasanna Gandhi (Member, IEEE) is with the Department of Mechanical Engineering, Indian Institute of Technology Bombay, Mumbai, India gandhi@iitb.ac.in

balances control effort and performance [8]. Given that full state feedback is typically unavailable in practical implementations, an observer is designed to estimate the unmeasured states [9]. The controller is validated through simulation and experimental implementation on a double parallelogram compliant mechanism. The results demonstrate that the controller effectively reduces transient response times, enhances disturbance rejection, and maintains stable oscillations with low computational effort, making it suitable for real-time applications.

II. Mathematical Model and Control Problem

The double parallelogram compliant mechanism is modeled as a two-mass spring-damper system, as shown in Fig. 1 [10].

The system parameters include:

- m_1: mass of the upper block
- m_2: mass of the lower block
- (k_1, c_1): stiffness and damping coefficient between m_1 and m_2
- (k_2, c_2): stiffness and damping coefficient between m_2 and the ground
- $u(t)$: external force applied to m_1 in the direction of displacement
- (x_1, x_2): displacements of m_1 and m_2

Defining the state vector as

$$x = \begin{bmatrix} x_1 & x_2 & \dot{x}_1 & \dot{x}_2 \end{bmatrix}^\top$$

the dynamic equations of the system are given by [6]

$$\dot{x} = A\,x + B\,u(t), \tag{1}$$

where the system matrices are

$$A = \begin{bmatrix} 0 & 0 & 1 & 0 \\ 0 & 0 & 0 & 1 \\ -\frac{k_1}{m_1} & \frac{k_1}{m_1} & -\frac{c_1}{m_1} & \frac{c_1}{m_1} \\ \frac{k_1}{m_2} & -\frac{k_1+k_2}{m_2} & \frac{c_1}{m_2} & -\frac{c_1+c_2}{m_2} \end{bmatrix}, B = \begin{bmatrix} 0 \\ 0 \\ \frac{1}{m_1} \\ 0 \end{bmatrix}. \tag{2}$$

Accurate parameter estimation is critical for constructing a reliable dynamic model. Experiments were performed to estimate the masses, spring constants, and damping coefficients. Details of these experiments are provided in the Appendix.

Using the values obtained from these experiments, the system matrices of the continuous-time state-space representation, as expressed in (1), and (2), are given by

$$A = \begin{bmatrix} 0 & 0 & 0.0010 & 0 \\ 0 & 0 & 0 & 0.0010 \\ -8442.5 & 730.0 & -0.2000 & 0.0000 \\ 1201.6 & -1201.6 & 0.1000 & -0.1000 \end{bmatrix}, \tag{3}$$

and

$$B = \begin{bmatrix} 0 \\ 0 \\ 2.5000 \\ 0 \end{bmatrix}. \tag{4}$$

III. Observer-Based LQR Controller Design

An observer-based LQR controller is developed to keep the system in resonant oscillation with transients dying down quickly. The control input is decomposed into two parts:

$$u(t) = v(t) + a\,\sin(\omega t), \tag{5}$$

where $u(t)$ is the total control input, a is a constant amplitude, and ω is a fixed frequency selected close to system's natural frequency to induce resonance. The LQR controller is applied only to the corrective component $v(t)$, which stabilizes the system around the desired resonant motion.

Since full-state feedback for LQR is not available in practical implementations, a state observer is used to estimate unmeasured states. To enable digital control, both the controller and the observer are designed in discrete time, avoiding the adverse effects of zero-order hold [11].

A. Discretization of the System

The continuous-time model in (1) is discretized with a sampling period T (here taken as 100μs). By defining:

$$x_k = x(kT), \quad v_k = v(kT), \quad t_k = kT,$$

and assuming a zero-order hold on $u(t)$ while approximating $\sin(\omega t) \approx \sin(\omega t_k)$ for $t \in [kT, (k+1)T)$, the following discrete-time model is obtained:

$$x_{k+1} = A_d\,x_k + B_d\Big(v_k + a\,\sin(\omega t_k)\Big), \quad y_k = C\,x_k, \tag{6}$$

with:

$$A_d = e^{AT}, \quad B_d = \int_0^T e^{A\tau} B\,d\tau. \tag{7}$$

This is consistent with standard digital control practice [11].

Substituting the values of matrices A and B in (7), we get

$$A_d = \begin{bmatrix} 0.9958 & 0.0004 & 0.0010 & 0.0000 \\ 0.0006 & 0.9994 & 0.0000 & 0.0010 \\ -8.4416 & 0.7299 & 0.9956 & 0.0004 \\ 1.2013 & -1.2016 & 0.0007 & 0.9993 \end{bmatrix}, \tag{8}$$

and

$$B_d = \begin{bmatrix} 0.0000 \\ 0.0000 \\ 0.0025 \\ 0.0000 \end{bmatrix}. \tag{9}$$

B. Decomposition via Superposition

Since (1) is linear with respect to x_k, the discrete state x_k can be decomposed into two components:

$$x_k = x_{a,k} + x_{b,k},$$

where:

Subsystem A (LQR Control Input Only):

$$x_{a,k+1} = A_d\,x_{a,k} + B_d\,v_k, \quad y_{a,k} = C\,x_{a,k},$$

Subsystem B (Sinusoidal Forcing Only):

$$x_{b,k+1} = A_d\,x_{b,k} + B_d\Big[a\,\sin(\omega t_k)\Big], \quad y_{b,k} = C\,x_{b,k}.$$

with $C = [0, 1, 0, 0]$ being the output matrix for this system.

Thus, the measured output becomes:

$$y_k = C\,x_k = y_{a,k} + y_{b,k}.$$

C. LQR Controller for Subsystem A

For Subsystem A, the following model is considered:

$$x_{a,k+1} = A_d\, x_{a,k} + B_d\, v_k.$$

The cost function J is defined as:

$$J = \sum_{k=0}^{\infty} \left[x_{a,k}^T\, Q\, x_{a,k} + v_k^T\, R\, v_k \right], \tag{10}$$

where $Q \succeq 0$ penalizes state deviations and $R \succ 0$ penalizes control effort. Solving Discrete Algebraic Riccati Equation (DARE) yields the optimal gain K [8], resulting in:

$$v_k = -K\, x_{a,k}.$$

The closed-loop dynamics are given by

$$x_{a,k+1} = (A_d - B_d\, K) x_{a,k},$$

which ensures convergence of $x_{a,k}$ to zero if (A_d, B_d) is stabilizable; i.e., there exist a gain K such that all eigenvalues of $(A_d - B_d K)$ lie strictly within the unit circle.

D. Forced Response of Subsystem B

The dynamics of Subsystem B are given by

$$x_{b,k+1} = A_d\, x_{b,k} + B_d\Big(a\, \sin(\omega t_k)\Big). \tag{11}$$

Under sinusoidal input, a discrete-time LTI system reaches a steady-state sinusoidal response of the same frequency [12]:

$$x_{b,k}^{(ss)} = a\, \big|H(e^{j\omega T})\big|\, \sin\Big(\omega t_k + \angle H(e^{j\omega T})\Big),$$

where the frequency response $H(e^{j\omega T})$ is

$$H(e^{j\omega T}) = \sum_{k=0}^{\infty} h(k)\, e^{-j\omega k T},$$

with $h(k)$ denoting the system's impulse response.

E. Error Convergence in Combined System

Without loss of generality, we assume that $x_{b,k}$ is in steady state since the initial time, i.e.,

$$x_{b,k} = x_{b,k}^{(ss)}.$$

Since $x_k = x_{a,k} + x_{b,k}$, the error can be defined as the deviation from the steady-state component, which comes out to be same as $x_{a,k}$.

$$\varepsilon_k = x_k - x_{b,k}^{(ss)} = x_k - x_{b,k} = x_{a,k}.$$

Substituting into the system dynamics,

$$x_{k+1} = A_d x_k + B_d\Big(v_k + a\, \sin(\omega t_k)\Big),$$

and using the steady-state dynamics of Subsystem B,

$$x_{b,k+1}^{(ss)} = A_d\, x_{b,k}^{(ss)} + B_d\Big(a\, \sin(\omega t_k)\Big),$$

we get the error dynamics:

$$\varepsilon_{k+1} = A_d\, \varepsilon_k + B_d\, v_k.$$

Since $\varepsilon_k = x_{a,k}$, LQR control (see Subsection III-C) can drive this error to zero rapidly, ensuring convergence of x_k to the desired steady-state $x_{b,k}^{(ss)}$.

F. Observer Design

As only the state x_2 is directly measured, a Luenberger observer is employed to estimate the full state vector:

$$\hat{x}_{k+1} = A_d\, \hat{x}_k + B_d\Big(u_k + a\, \sin(\omega t_k)\Big) + L\Big(y_k - C\, \hat{x}_k\Big), \tag{12}$$

where $\hat{x}_k$ is the estimated state vector, $e_k = x_k - \hat{x}_k$ is state estimation error, and L is selected such that error dynamics,

$$e_{k+1} = (A_d - L\, C) e_k,$$

are stable. For stability, the eigenvalues of $A_d - LC$ must lie strictly within the unit circle [9].

G. Observer Gain Selection and LQR Controller Design

It was observed that direct placement of observer poles in the discrete-time domain led to large numerical sensitivity, with minor perturbations in L (on the order of 10^{-4} to 10^{-5}) leading to instability. This was not okay for practical application on microcontroller. To improve robustness, desired observer poles were first selected in the continuous-time domain and then mapped to discrete time using:

$$z_i = \exp(\lambda_i T),$$

where T is the sampling period. MATLAB's `place` function was used to compute the corresponding observer gain matrix L [13]. The chosen poles were:

$$\lambda_{\text{cont}} = \{-50 \pm j, -300 \pm 2j\}.$$

This resulted in a robust gain:

$$L = \begin{bmatrix} 2.0832 \\ 0.6060 \\ -604.4909 \\ 103.5684 \end{bmatrix}, \tag{13}$$

which ensures stable state estimation across sampling times from 1 μs to 5 ms, and is robust to numerical precision limitations in practical implementation.

The LQR controller was designed using:

$$Q = \text{diag}([1, 500, 100, 5000]), \quad R = 50.$$

The discrete-time gain matrix K_{lqr} was computed by solving the DARE using MATLAB's `dlqr` function, resulting in:

$$K_{\text{lqr}} = \begin{bmatrix} 12.9757 & -14.3664 & 3.6105 & 9.4883 \end{bmatrix}. \tag{14}$$

These controller parameters ensure optimal regulation by minimizing a standard quadratic cost function while respecting the physical constraints of the system, including the actuator force limit of 4 N and permissible state bounds. It also achieves the required oscillation amplitudes of at least 5 mm, enabling the end mass to attain the desired near-straight motion of 1 cm, thereby fulfilling its intended objective.

IV. Simulation Study

A series of simulations were performed to evaluate the performance of the proposed observer-based LQR controller. Simulations were conducted using MATLAB 2024a on Windows 11, incorporating realistic disturbances, sensor noise, and calibration errors to rigorously evaluate the controller's robustness.

The simulations parameters to reflect realistic system:

- Sampling time T_s: 0.1 ms
- Input frequency w: 30 Hz (natural frequency: 32.71 Hz)
- Input sine amplitude a: 3 N
- State bounds for x_1 and x_2: $[-15, +15]$ mm
- Maximum actuator force: 4 N
- Target amplitude of x_2: slightly greater than 5 mm (To create a near-straight motion of 1 cm for the end mass)

A. Settling Time Analysis

Fig. 2 shows that under pure sinusoidal excitation without feedback, transients persist for more than 100 seconds. In contrast, the proposed control strategy (Fig. 3) achieves steady-state in under 3 seconds, demonstrating substantial improvement.

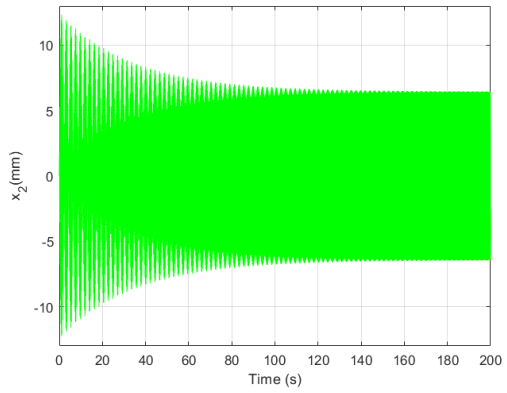

Fig. 2. State x_2 versus time with only primary sinusoidal excitation

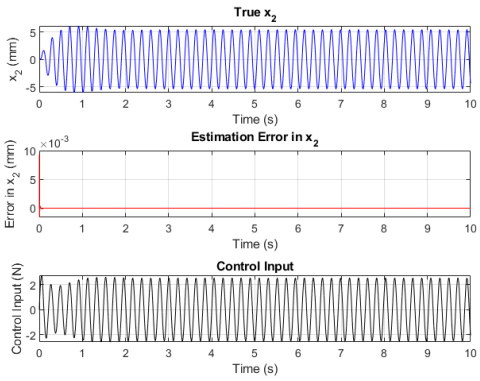

Fig. 3. True state x_2, estimation error, and control input versus time using the proposed control strategy

B. Disturbance Rejection

To evaluate disturbance rejection, random disturbances were added to the system:

$$X_{k+1} = A_d X_k + B_d\big(v_k + a\sin(wt_k) + \text{disturbance}_k\big),$$

with observer dynamics unchanged:

$$\hat{X}_{k+1} = A_d\hat{X}_k + B_d\big(v_k + a\sin(wt_k)\big) + L(C_d Y_k - C_d\hat{X}_k).$$

As shown in Fig. 4, the controller maintains robust performance despite disturbances.

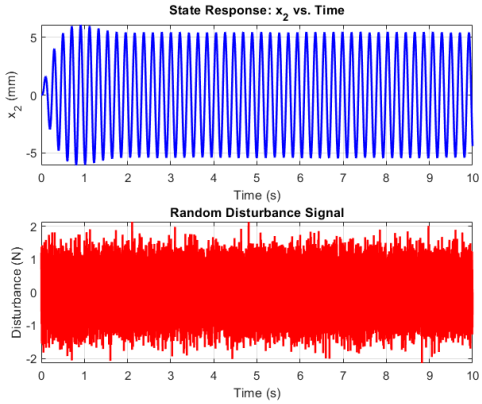

Fig. 4. State x_2 with disturbance versus time using the proposed control strategy

C. Noise Robustness

Simulations with sensor noise up to 2 mm confirm that the controller maintains performance, as illustrated in Fig. 5.

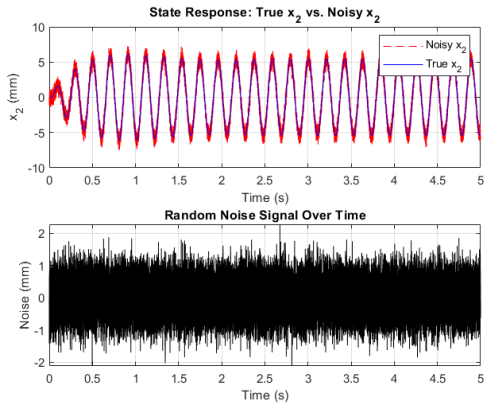

Fig. 5. State x_2 with noise versus time using the proposed control strategy

D. Calibration Error Sensitivity

To mimic sensor miscalibration, a constant offset, unlike zero-centered random noise, was introduced in the sensor reading. Even with an unreasonable 2 mm offset (Fig. 6), the controller still stabilized the system with a slight steady-state shift. In real scenarios, where errors are in orders of micrometers, this shift is negligible.

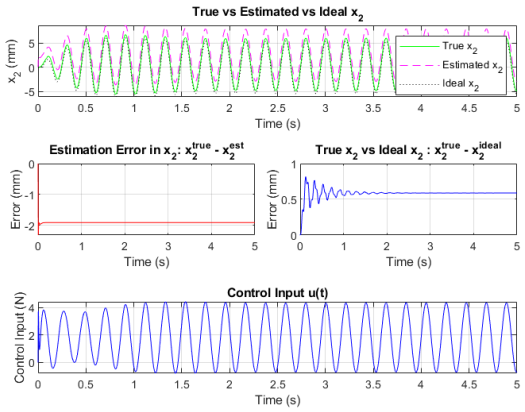

Fig. 6. Comparison of true, estimated, and ideal x_2 versus time under high sensor calibration error (2 mm) using the proposed control strategy

V. Experimental Implementation on STM32

The proposed controller and observer were implemented on an STM32F429ZITx Discovery Board to verify real-time performance. A sampling period of T_s = 0.1 ms, consistent with the simulations, was used. A voice coil actuator with a force limit of 4 N and a linear encoder with a resolution of 1 μm were employed. Although the control design was based on simplified two-mass spring-damper system, the controller is actually implemented on a highly nonlinear large deformation double parallelogram compliant mechanism.

While the convergence time is affected by the deviations between the linear design model and the real nonlinear system, the proposed controller consistently maintained stability during the experiments, highly reducing the transient duration, while also adding robustness to disturbances.

A. Real-Time Performance

The computation time for each control iteration, from sensor acquisition to PWM generation, is measured using digital I/O pins of the STM32 microcontroller to be approximately 30 μs, which is only a small fraction of the 0.1 ms sampling interval and is suitable for real-time applications.

B. Implementation Details

A hardware timer was configured to trigger an interrupt every 0.1 ms. Within the interrupt service routine, the observer update is performed as:

$$\hat{x}_{k+1} = A_d\,\hat{x}_k + B_d\Big(u_k + a\,\sin(\omega t_k)\Big) + L\Big(y_k - C\,\hat{x}_k\Big),$$

and the control law is applied using:

$$u_k = -K\,\hat{x}_k.$$

The computed control signal u_k is converted into a PWM signal, with direction being determined by the sign of u_k.

C. Experimental Results

The plot shown in Fig. 7 was generated using the real-time data acquired by dSPACE ControlDesk 5.2. This plot demonstrates displacement x_2 under the proposed control algorithm.

The experimental system exhibits significant nonlinear behavior and parameter uncertainties, resulting in deviations from the simplified linear model used during controller design. Despite these challenges, the proposed controller demonstrates a substantial improvement in performance, reducing the settling time from 100+ seconds to around 15 seconds.

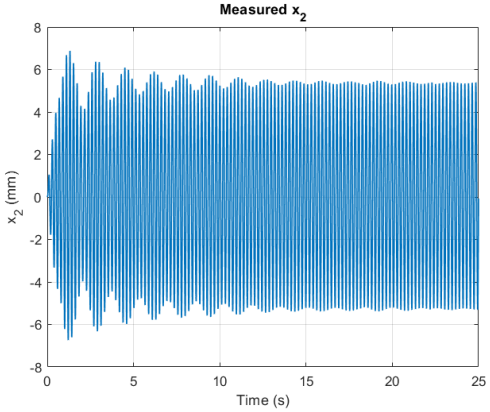

Fig. 7. Experimental measurement of x_2 versus time using the proposed control algorithm

VI. Conclusion

An observer-based LQR controller has been developed to maintain resonant oscillations in a non-colocated double parallelogram compliant mechanism while ensuring rapid transient suppression. This method distinguishes itself from approaches that depend exclusively on pure feedforward control with output error feedback, or that necessitate heavy computations unsuitable for real-time applications. By decomposing the control input into two components $u(t) = v(t) + a\,\sin(\omega t)$, that is, a primary excitation signal and an LQR-based corrective signal, the proposed strategy achieves a drastic reduction in settling time. Moreover, this controller proved to be highly robust for disturbances and noise, all without imposing high computational demands. This approach has been rigorously validated through comprehensive simulation studies and successful real-time implementation on an STM32 microcontroller, showing the potential of this control algorithm to be useful in a wide range of real-time applications.

Appendix

Accurate parameter estimation is critical for constructing a reliable dynamic model. Experiments were performed to estimate masses, spring constants, and damping coefficients.

A. Mass Measurements

The masses of both the blocks were measured using a weighing scale. The measured values were:

$$m_1 = 400\,\text{g}, \quad m_2 = 243\,\text{g}.$$

B. Estimation of Spring Constants

The spring constants k_1 and k_2 were estimated using controlled deflection experiments.

For k_1, calibrated weights were suspended from m_1 using a light string and a low-friction pulley such that the compliant beams between m_1 and m_2 were not affected. This configuration replicates the bending of compliant beams when a perpendicular load is applied, as described in [6].

To estimate k_2, m_1 was rigidly constrained and calibrated weights were attached to m_2, isolating the spring connecting m_1 and m_2.

The resulting displacement versus load measurements for both experiments were plotted to find values of k_1 and k_2 to be 3085 N/m and 292 N/m respectively.

C. Estimation of Damping Coefficients

Damping coefficients were determined by analyzing the free-vibration decay of the system. With m_1 constrained, m_2 was allowed to oscillate freely. The natural frequency (ω_{nc}), damped frequency (ω_{dc}), and logarithmic decrement (δ_c) were extracted from the oscillations. The experimentally determined parameters with and without constraining m_1 are summarized in Table I and Table II. The damping ratio (ζ_c) was computed using: [15]

$$\zeta_c = \frac{\delta_c}{\sqrt{4\pi^2 + \delta_c^2}},$$

and the damping coefficient c_2 was then calculated as:

$$c_2 = 2\zeta_c m_2 \omega_{nc}.$$

This resulted in c_2 = 0.0166 kg/s.

TABLE I

EXPERIMENTAL DAMPING AND STIFFNESS PARAMETERS (RIGIDLY CONSTRAINED m_1)

Parameter	Estimated Value
Logarithmic Decrement (δ_c)	0.0061059
Damping Ratio (ζ_c)	0.00097178
Damped Frequency (ω_{dc})	35.2792 rad/s
Natural Frequency (ω_{nc})	35.2792 rad/s
Effective Stiffness (k_{ec})	301.1987 N/m

TABLE II

EXPERIMENTAL DAMPING AND STIFFNESS PARAMETERS (UNCONSTRAINED m_1)

Parameter	Estimated Value
Logarithmic Decrement (δ_u)	0.00598
Damping Ratio (ζ_u)	0.00095
Damped Frequency (ω_{du})	32.71 rad/s
Natural Frequency (ω_{nu})	32.71 rad/s
Effective Stiffness (k_u)	258.93 N/m

Additionally, c_1 was estimated to be 0.07 kg/s using

$$c_1 = 2\zeta\sqrt{m_1 k_2},$$

where ζ is considered as the average of ζ_c and ζ_u because, as shown in Table I and Table II, the values of the damping coefficient across the system exhibit minimal deviation (less than 3%). Hence, the estimated value of c_1 is approximately 0.07 kg/s, with a deviation of up to 5%, which is acceptable for this application.

D. Discussion

The experimental results for the spring constant k_2 found using controlled deflection experiments are in close agreement with theoretical predictions (k_{ec}) made from the free-vibration decay experiment with constrained m_1. The consistency across different experimental methods reinforces the reliability of the parameter estimates.

REFERENCES

[1] Pengwang, Eakkachai, Rabenorosoa, Kanty, Rakotondrabe, Micky, and Andreff, Nicolas, "Scanning Micromirror Platform Based on MEMS Technology for Medical Application," *Micromachines*, vol. 7, p. 24, 2016, doi:10.3390/mi7020024.

[2] S. Deshmukh and P. S. Gandhi, "Optomechanical scanning systems for microstereolithography (MSL): Analysis and experimental verification," *J. Mater. Process. Technol.*, vol. 209, no. 3, pp. 1275–1285, 2009, doi:10.1016/j.jmatprotec.2008.03.056.

[3] X. Sun, W. Chen, R. Zhou, J. Zhang, and W. Chen, "Design of compliant parallel mechanism for Nanoimprint Lithography," in *Proc. IEEE Int. Conf. on Nanoimprint Lithography*, Beijing, China, 2011, pp. 1–6.

[4] S. Lin, Y. Jia, I. P. Lei, and Q. Xu, "Design and Optimization of a Long-Stroke Compliant Micropositioning Stage Driven by Voice Coil Motor," in *Proc. 12th Int. Conf. Control Autom. Robot. Vis. (ICARCV)*, Guangzhou, China, Dec. 2012, pp. 1717–1720, doi:10.1109/ICARCV.2012.

[5] B.-Z. Guo, J.-M. Wang, and K.-Y. Yang, "Dynamic stabilization of an Euler–Bernoulli beam under boundary control and non-collocated observation," *Systems and Control Letters*, vol. 57, no. 9, pp. 740–749, Sep. 2008, doi:10.1016/j.sysconle.2008.02.004.

[6] S. S. Rao, *Mechanical Vibrations*, 5th ed. Pearson, 2011.

[7] M. B. Akbarzadeh, H. Moeenfard, and S. Awtar, "Nonlinear dynamic modeling of a parallelogram flexure," *Mech. Mach. Theory*, vol. 151, p. 103908, Jul. 2020.

[8] M. Rodrigues, G. Moreira, and E. L. K. Hemerly, "Nonlinear LQR Control for Underactuated Mechanical Systems," *IFAC-PapersOnLine*, vol. 51, no. 3, pp. 171–176, 2018, doi:10.1016/j.ifacol.2018.06.318.

[9] P. S. Shiakolas and D. Piyabongkarn, "Development of a Real-Time Digital Control System with a Hardware-in-the-Loop Magnetic Levitation Device for Reinforcement of Controls Education," *IEEE Trans. Educ.*, vol. 46, no. 1, pp. 79–87, Feb. 2003, doi:10.1109/TE.2002.808268.

[10] T. Abhijit and G. Prasanna, "Design and Analysis of Ultra-Precise Large Range Linear Motion Platforms Using Compliant Mechanism," *IEEE Access*, vol. 10, pp. 94321–94336, 2022, doi:10.1109/ACCESS.2022.3201343.

[11] K. J. Åström and B. Wittenmark, *Computer-Controlled Systems: Theory and Design*, 3rd ed. Mineola, NY, USA: Dover Publications, 2011.

[12] H. Balakrishnan, C. Terman, and G. Verghese, "Chapter 12: Frequency Response of LTI Systems," in *Bits, Signals, and Packets: An Introduction to Digital Communications and Networks*, Massachusetts Institute of Technology, Fall 2012. [Online]. Available: https://ocw.mit.edu/...chap12/. [Accessed: Apr. 6, 2025].

[13] The MathWorks, Inc., "place," MATLAB Control System Toolbox Documentation, [Online]. Available: `https://in.mathworks.com/help/control/ref/place.html`. [Accessed: Mar. 7, 2025].

[14] The MathWorks, Inc., "dlqr," MATLAB Control System Toolbox Documentation, [Online]. Available: `https://in.mathworks.com/help/control/ref/dlqr.html`. [Accessed: Mar. 7, 2025].

[15] L. Meirovitch, *Fundamentals of Vibrations*. New York, NY, USA: McGraw-Hill, 1986.